

Improved Electronic Structure and Optical Performance of $\text{Bi}_2\text{Te}_{3-x}\text{Se}_x$ From First-principle Calculations Within TB-mBJ Exchange Potential

Berber Mohamed^{a,*}, Mokaddem Allel^{a,b}, Doumi Bendouma^c, Boutaleb Miloud^c, Medjahed Baghdad^d

^aInstitute of Technology, Nour Bachir University Center, El-Bayadh, 32000, Algeria.

^bTheoretical Physics Laboratory, U.S.T.H.B, Algiers, Algeria

^cPhysics Department, Faculty of Sciences, University Dr Moulay Tahar, Saida, Algeria.

^dLaboratory of Separation and Purification Technology, Department of Chemistry, Faculty of Sciences, Tlemcen University, Algeria

Received: February 09, 2017; Revised: September 18, 2017; Accepted: October 05, 2017

Using the first-principle calculations of density functional theory within the (FP-LAPW) method, we have investigated the structural, electronic and optical properties of $\text{Bi}_2\text{Te}_{3-x}\text{Se}_x$ alloys with compositions $x = 0, 1, 2$ and 3 of Se. The generalized gradient approximation functional of Wu and Cohen (GGA-PBE) is used to calculate ground state structural parameters of $\text{Bi}_2\text{Te}_{3-x}\text{Se}_x$, which are in good agreement with theoretical and experimental data. The electronic band structures and optical constants have been improved with Tran-Blaha modified Becker-Johnson (TB-mBJ) parameterization scheme. Also, we have analyzed in detail the performance of dielectric function, refractive index, reflectivity and optical conductivity of these alloys. Our results show that $\text{Bi}_2\text{Te}_{3-x}\text{Se}_x$ alloys are promising candidates for optoelectronic applications especially in the Infrared and visible fields. $\text{Bi}_2\text{Te}_{3-x}\text{Se}_x$ materials have a direct band gap and can be tuned from 0.1706 eV to 0.7819 eV by varying In composition so emission was tunable from 1.58 to 7.26 micrometers (infrared field), in addition for their direct band gap and in view of their attractive optical properties such conductivity, absorption and reflectivity these materials is considered as promising materials for optoelectronic applications.

Keywords: First-principle calculations, TB-mBJ, Electronic structure, Optical properties.

1. Introduction

Bismuth telluride (Bi_2Te_3) and bismuth selenide (Bi_2Se_3) have technological interest owed to their thermoelectric utilization, narrow band gap and photosensitive¹. During last decennaries, these compounds have been extensively studied to advance their thermoelectric and optical properties by different aspect technological like doping, high-pressure and variation in mesostructure²⁻⁵. Structural, electrical and optical properties of Bi_2Se_3 and $\text{Bi}_2\text{Se}_{(3-x)}\text{Te}_x$ thin films have been studied experimentally⁶. Synthesis and thermoelectric characterization of Bi_2Te_3 nanoparticles has been studied experimentally⁷. Yamini Sharma et al.⁸ have studied the electronic structure, optical properties and Compton profiles of Bi_2S_3 and Bi_2Se_3 . Oriented Bi_2Se_3 nanoribbons film: Structure, growth, and photoelectric properties have been studied experimentally by Yuan Yu et al.⁹. Thermoelectricity and superconductivity in pure and doped Bi_2Te_3 with Se is reported by H.A. Rahnamaye Aliabad and M. Kheirabadi¹⁰. Recently Kun Zhao et al. have calculated the pressure-induced anomalies in structure, charge density and transport properties of Bi_2Te_3 using density functional theory (DFT) in the framework of the projector augmented waves method¹¹.

Preceding studies have reported that Bi_2Te_3 , $\text{Bi}_2\text{Te}_2\text{Se}$, Bi_2TeSe_2 and Bi_2Se_3 , crystallizes in hexagonal crystal with

the space group $\text{hR}5$ ($\text{R}3\text{m}$)¹² as demonstrated in Fig. 1. The structures can be detected as Bi and Te (Se) layers stacked along the c-axis and containing five atoms per unit cell (two Bi atoms and three Te or Se atoms)¹⁰. Increase both theoretical and experimental investigation on electronic structure and optical properties of $\text{Bi}_2\text{Te}_{3-x}\text{Se}_x$ ($x=0,1,2$ and 3) exhibit a direct band gap¹³ and The refractive index of the Bismuth Telluride is higher than any value previously reported for a semiconductor¹⁴.

In this work the principle of our inspection is concentrated on predicting the structural, electronic and optical properties of $\text{Bi}_2\text{Te}_{3-x}\text{Se}_x$ alloys with a number of concentrations (x) ($x=0,1,2$ and 3). We have used in this calculation the full potential linearized augmented plane wave (FP-LAPW) method within density functional theory (DFT)¹⁵. For theoretical calculations of structural constants we used the generalized gradient approximation GGA with PBE functional¹⁶ for electronic and optical properties we used Tran-Blaha modified Becke-Johnson exchange potential approximation (TB-mBJ)¹⁷.

After the abstract and introduction, the rest of the paper is formed as follows: in Section 2, a brief outline of the method of calculation is given. In Section 3 details of the obtained results and discussion related to structural, electronic and optical properties of $\text{Bi}_2\text{Te}_{3-x}\text{Se}_x$ alloys are presented. The

*e-mail: berber.mohamed16@gmail.com

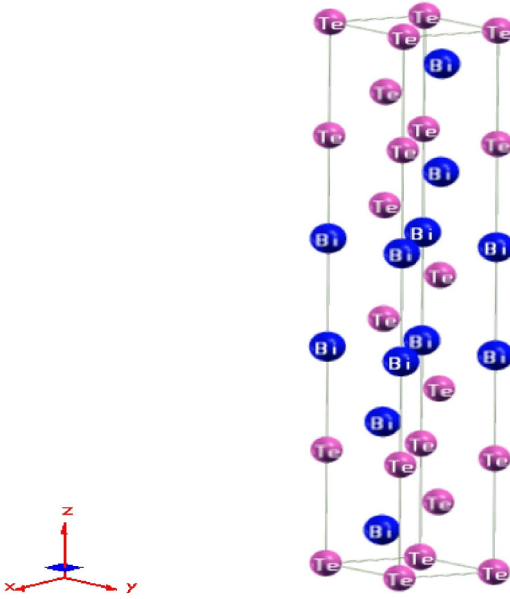


Figure 1. The crystal structure of Bi₂Te₃.

main conclusions of our present work are summarized in Section 4.

2. Method of Calculation

In the present study, we have used the (FP) full-potential (LAPW) linearized augmented plane wave (FP-LAPW) method within the framework of the density functional theory (DFT) ¹⁵ as implemented in the Wien2k code ¹⁸. In calculating structural parameters, we have used the generalized gradient approximation (GGA) with PBE functional because Numerical tests have shown that the PBE-GGA gives total-energy dependent properties in good agreement with experiment ¹⁹⁻²⁰.

(GGA-BPE) ¹⁶ and the recently recommended and better predictable approach technique called Tran-Blaha modified Becker-Johnson (TB-mBJ) potential approximation ¹⁷ have been used to calculate electronic and optical properties of Bi₂Te_{3-x}Se_x by reason it is capable to illustrate correctly the electronic structure of the solids and the insulators ^{21,22,23}. Tran et al., have demonstrated that this form of approach develop over the GGA and LDA potentials for the determination of band gaps value ²⁴.

In this paper, we have selected the muffin-tin radii (MT) for each atoms (Bi, Te and Se) to be 2.50 atomic units (a.u.). The $K_{\max} = 8 \text{ (RMT)}^{-1}$ (Kmax is the plane wave cut-off and RMT is the smallest of all atomic sphere radii). The Fourier expanded charge density was truncated at $G_{\max} = 12 \text{ (Ryd)}^{1/2}$, the l-expansion of the non-spherical potential and charge density was carried out up to $l_{\max} = 10$. The cut-off energy is set to -6 Ryd to isolate core from valence states. The self-

consistent calculations are evaluated to be converged when the total energy of the system is stable within 0.0001 Ryd.

3. Results and Discussion

3.1. Structural properties

With a view to calculate the ground states properties of Bi₂Te₃, Bi₂Te₂Se, Bi₂TeSe₂ and Bi₂Se₃ the total energies are calculated for different volumes about the equilibrium cell volume V_0 . The calculated total energies are adapted to the Murnaghan's equation of state ²⁵ to find the ground state properties like the equilibrium lattice constant a , c , the bulk modulus B and its pressure derivative B' . The calculated equilibrium parameters (a , c , B and B') for all structures are given in Table 1, which also contains works of previous calculations as well as the experimental data. Previous research have reported that Bi₂Te₃, Bi₂Te₂Se, Bi₂TeSe₂ and Bi₂Se₃, have the greatest possibility of crystallizing in trigonal system (hexagonal) with the space group $R\bar{3}m$ ($N^\circ 166$) and in orthorhombic system with the space group $Pnma$ ($N^\circ 62$).

In Fig. 2, we depicted the calculated lattice constants a and c as a function of selenide concentration (x) ($x=0,1,2$ and 3) and with comparative data ¹⁰. We have determined the total bowing parameter (b) by fitting the non linear variation optimized lattice constants a and c as Se concentration (x) by the quadratic function. Our results are presented by the relation (1) and that comparative data ¹⁰ are presented with the relation (2).

$$\begin{cases} a_{Bi_2Te_{3-x}Se_x}^{GGA-PBE} = 4.38327 - 0.05543x - 0.00975x^2 \\ c_{Bi_2Te_{3-x}Se_x}^{GGA-PBE} = 30.1716 - 0.76135x + 0.04175x^2 \end{cases} \quad (1)$$

$$\begin{cases} a_{Bi_2Te_{3-x}Se_x}^{GGA-PBE(Ref.10)} = 4.38071 + 0.00341x - 0.00075x^2 \\ c_{Bi_2Te_{3-x}Se_x}^{GGA-PBE(Ref.10)} = 30.53992 - 0.04759x + 0.01045x^2 \end{cases} \quad (2)$$

Our results exhibit a negligible bowing parameter for the lattice constant a which has a bowing parameter $b = 0.00442 \text{ \AA}$ and $b = 0.01233 \text{ \AA}$ for the lattice constant c .

The bulk modulus of Bi₂Te_{3-x}Se_x for various x concentrations is reported in Table 1. The variation of the bulk modulus versus Se composition (x) is presented in Fig. 3 the bowing parameter of the bulk modulus is determined by fitting the non linear variation, Relation (3) exhibit the result:

$$B_{Bi_2Te_{3-x}Se_x}^{GGA-PBE} = 54.89137 + 2.44141x + 0.50583x^2 \quad (3)$$

3.2. Electronic properties

In this part, we have calculated the electronic band structure for Bi₂Te_{3-x}Se_x using GGA-PBE ¹⁶ and (TB-mBJ) of Tran-Blaha modified Becke-Johnson ¹⁷ approaches.

Table 2, show the computed energy band gaps E_g of Bi₂Te_{3-x}Se_x using (GGA-PBE) and (TB-mBJ) approaches

Table 1. Lattice constants a (in Å), c (in Å), bulk modulus B (in GPa) and its pressure derivative B' of $\text{Bi}_2\text{Te}_{3-x}\text{Se}_x$ with their corresponding experimental values and other theoretical data.

| Compound | Present work GGA-PBE | | | | Other work | | | |
|---|----------------------|---------|---------|--------|---|--|-----|------|
| | a | c | B | B' | a | c | B | B' |
| $\text{Bi}_2\text{Te}_{3-x}\text{Se}_x$ x | | | | | | | | |
| 0 | 4.4750 | 30.3334 | 45.9108 | 4.5049 | 4.37 ^a , 4.38 ^b , 4.36 ^c , 4.38 ^d , 4.38029 ^e | 30.34 ^a , 30.49 ^b , 30.38 ^c , 30.44 ^d , 30.54569 ^e | - | - |
| 1 | 4.4180 | 29.2869 | 49.2575 | 4.8404 | 4.283 ^d , 4.38462 ^e | 29.846 ^d , 30.48549 ^e | - | - |
| 2 | 4.2753 | 29.4326 | 52.6106 | 4.8990 | 4.38328 ^e | 30.50385 ^e | - | - |
| 3 | 4.2006 | 28.4354 | 57.7929 | 4.5178 | 4.14 ^e , 4.13 ^f , 4.38461 ^g | 28.64 ^e , 28.48 ^f , 30.48545 ^g | - | - |

a^[26] Experiment;

b^[27] Experiment;

c^[28] Theory;

d^[29] Experiment;

e^[30] Experiment;

f^[31] Experiment;

g^[10] Theory;

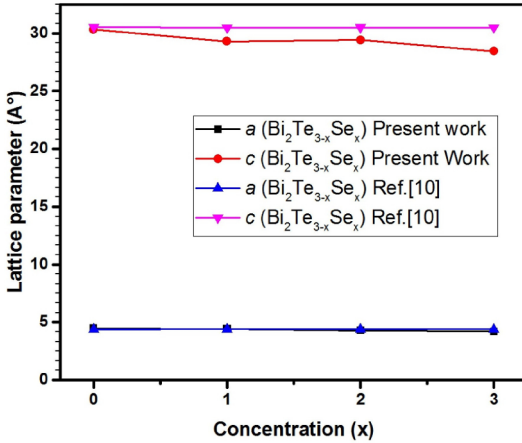
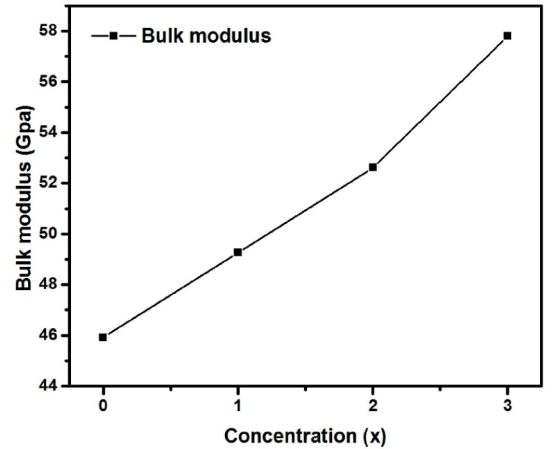

Figure 2. Calculated lattice constant a and c of $\text{Bi}_2\text{Te}_{3-x}\text{Se}_x$ as a function of Se concentration (x).

Figure 3. The variation of the bulk modulus of $\text{Bi}_2\text{Te}_{3-x}\text{Se}_x$ versus Se composition (x)

Table 2. Energy band gaps E_g (eV) for $\text{Bi}_2\text{Te}_{3-x}\text{Se}_x$ alloys using (GGA-PBE) and (TB-mBJ) schemes and their corresponding experimental and theoretical data.

| Compound | x | Present work | | Other work | |
|---|-----|--------------|--------|---|--|
| | | GGA-PBE | TB-mBJ | Theoretical | Experimental |
| $\text{Bi}_2\text{Te}_{3-x}\text{Se}_x$ | x | | | | |
| | 0 | 0.29333 | 0.4868 | (0.12- 0.28) ^g , 0.154 ^m , 0.11 ⁿ | 0.11h, 0.16 ^j |
| | 1 | 0.07261 | 0.1706 | (0.18-0.04) ^g | |
| | 2 | 0.70175 | 0.7819 | (0.22- 0.52) ^g | |
| | 3 | 0.32005 | 0.5241 | (0.20- 0.32) ^g | (0.2-0.3) ^k , 0.56 ^l |

g^[10] Theory;

h^[32] Experiment;

i^[33] Experiment;

j^[34] Experiment;

k^[35, 36] Experiment;

l^[8] Experiment;

m^[37] Theory;

n^[38] Theory;

for all studied composition (x) ($x=0,1,2$ and 3), theoretical data for all concentration¹⁰ and experimental data only for Bi_2Te_3 and Bi_2Se_3 . Fig. 4 shows the variation of band gap energies E_g versus the concentration (x) for the $\text{Bi}_2\text{Te}_{3-x}\text{Se}_x$ compared with other theoretical calculation of band gap with and without spin orbit coupling (SOC)¹⁰.

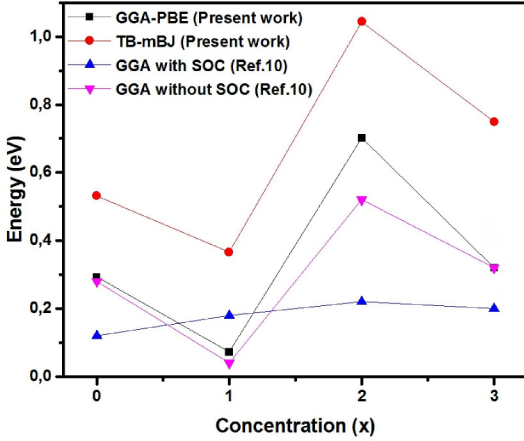


Figure 4. The variation of band gap energies E_g of $\text{Bi}_2\text{Te}_{3-x}\text{Se}_x$ versus the concentration (x).

The electronic band structures properties were determined for all structures with the predicted lattice constant via GGA-PBE and TB-mBJ approaches. However, the results obtained by TB-mBJ approach and GGA-PBE are plotted. Fig. 5 shows the electronic band structures calculated for along the high-symmetry lines of the first Brillouin zone. The valence band maximum (VB_{max}) and conduction band minimum (CB_{min}) are founded Γ at point, showing $\text{Bi}_2\text{Te}_{3-x}\text{Se}_x$ have the direct band gap for all concentration (x) ($x=0,1,2$ and 3), which are satisfactory for optoelectronic materials.

3.3. Optical properties

The frequency dependent complex dielectric function $\varepsilon(\omega)=\varepsilon_1(\omega)+i\varepsilon_2(\omega)$ is admitted to define the optical reply of the medium at all photon $E=\hbar\omega$. wherever $\varepsilon_1(\omega)$ and $\varepsilon_2(\omega)$ are the real (dispersive) and the imaginary (absorptive) parts of $\varepsilon(\omega)$ respectively.

The imaginary part of the dielectric function, $\varepsilon_2(\omega)$ is obtained from the momentum matrix elements⁴⁰, and the electronic structure calculation (densities of states). The real part $\varepsilon_1(\omega)$ can be derived from the $\varepsilon_2(\omega)$, using the Kramer-Kronig transformations⁴¹. The imaginary part of the dielectric function $\varepsilon_2(\omega)$ is expressed as follows:

$$\varepsilon_2(\omega) = \frac{4\pi e^2}{\Omega \varepsilon_0} \sum_{k,v,c} |\langle \varphi_k^c | u_x r | \varphi_k^v \rangle|^2 \delta(E_k^c - E_k^v - \hbar\omega) \quad (4)$$

where e is the electric charge, Ω is the unit cell volume, u is the vector defining the polarization of the incident electric field, ω is the frequency of the light, φ_k^c and φ_k^v are the wave

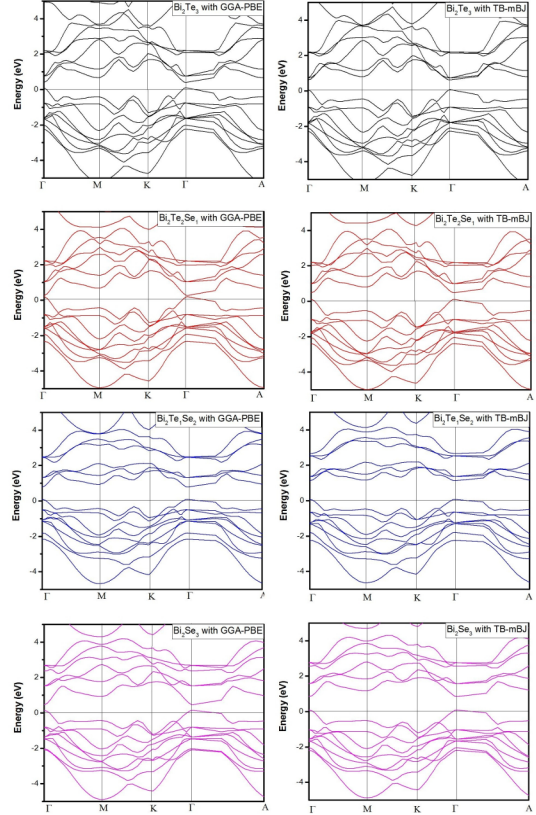


Figure 5. Band structure calculated for $\text{Bi}_2\text{Te}_{3-x}\text{Se}_x$ using (TB-mBJ) method and GGA-PBE.

functions of the conduction and valence bands, respectively. The real part of the dielectric function can be evaluated from $\varepsilon_2(\omega)$ using the Kramers-Kronig relations is given by:

$$\varepsilon_1(\omega) = 1 + \frac{2}{\pi} P \int_0^{\infty} \frac{\omega' \varepsilon_2(\omega')}{\omega'^2 - \omega^2} d\omega' \quad (5)$$

The knowledge of both the real and imaginary parts of the dielectric function allows the calculation of important optical functions such as the refractive index $n(\omega)$, extinction coefficient $k(\omega)$, absorption coefficient $\alpha(\omega)$, optical conductivity $\sigma(\omega)$, loss energy function $L(\omega)$ and the reflectivity $R(\omega)$ ⁴²⁻⁴⁴.

$$n(\omega) = \frac{1}{\sqrt{2}} [(\varepsilon_1^2 + \varepsilon_2^2)^{1/2} + \varepsilon_1]^{1/2} \quad (6)$$

$$K(\omega) = \frac{1}{\sqrt{2}} [(\varepsilon_1^2 + \varepsilon_2^2)^{1/2} - \varepsilon_1]^{1/2} \quad (7)$$

$$\alpha(\omega) = \sqrt{2\omega} \frac{1}{\sqrt{2}} [(\varepsilon_1^2 + \varepsilon_2^2)^{1/2} - \varepsilon_1]^{1/2} \quad (8)$$

The conductivity and the dielectric constant are related to each other by the relation:

$$\varepsilon(\omega) = 1 + \left(\frac{4\pi i}{\omega} \right) \sigma(\omega). \quad (9)$$

According to the Drude classical free-electron theory $\epsilon''(\omega)$ is given by the relation

$$\sigma(\omega) = \frac{N_c e^2}{m_{\text{eff}}} \frac{\omega'}{\omega^2 + \omega'^2} \quad (10)$$

The loss function $L(\omega)$ which is also an important optical parameter describing the energy loss of a fast electron traversing in the material, can be calculated from the dielectric constant as:

$$L(\omega) = -\text{Im} \left[\frac{1}{\epsilon(\omega)} \right] = \frac{\epsilon_2(\omega)}{\epsilon_1^2(\omega) + \epsilon_2^2(\omega)} \quad (11)$$

The reflectivity is calculated from the following relation:

$$R(\omega) = \left| \frac{\sqrt{\epsilon_1(\omega) + i\epsilon_2(\omega)} - 1}{\sqrt{\epsilon_1(\omega) + i\epsilon_2(\omega)} + 1} \right|^2 \quad (12)$$

In order to calculate the optical properties, one needs to use a dense mesh of uniformly distributed k -points. We present calculations with 120 k -points in this study.

The calculated optical parameters for radiation up to 20 eV, within the TB-mBJ approach, are presented in Figs. 6-16.

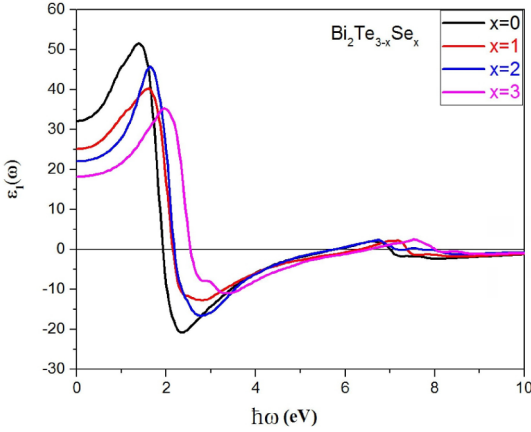


Figure 6. The real parts of the dielectric function for $\text{Bi}_2\text{Te}_{3-x}\text{Se}_x$ ($x=0, 1, 2$ and 3)

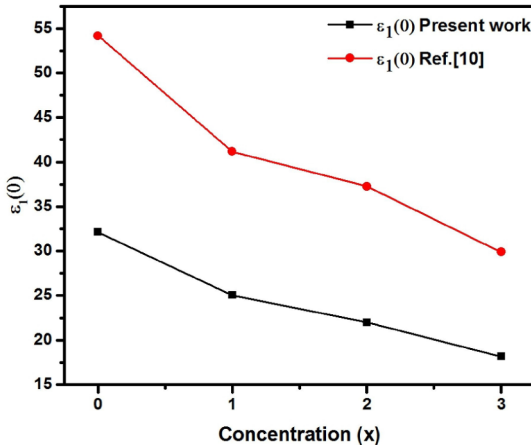


Figure 7. The static dielectric constants $\epsilon_1(0)$ of $\text{Bi}_2\text{Te}_{3-x}\text{Se}_x$ versus concentration (x).

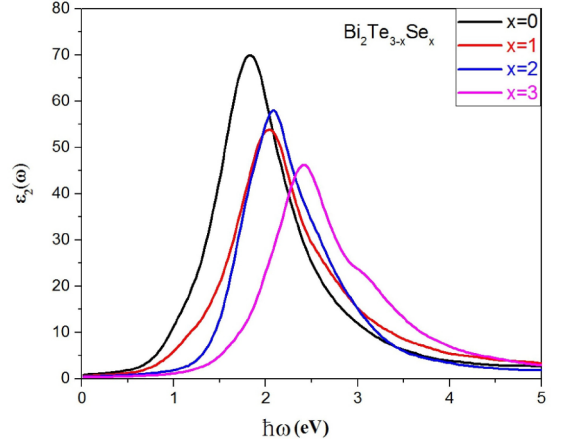


Figure 8. Calculated imaginary parts of the dielectric function of $\text{Bi}_2\text{Te}_{3-x}\text{Se}_x$ ($x=0, 1, 2$ and 3).

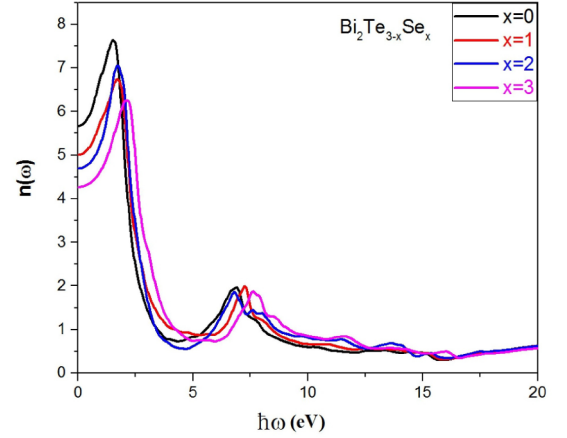


Figure 9. The refractive index n of $\text{Bi}_2\text{Te}_{3-x}\text{Se}_x$

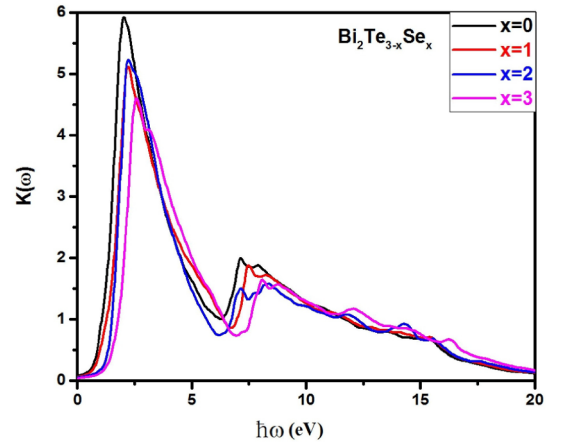


Figure 10. The extinction coefficient K of $\text{Bi}_2\text{Te}_{3-x}\text{Se}_x$

Fig. 6 shows the real part of the dielectric function for $\text{Bi}_2\text{Te}_{3-x}\text{Se}_x$ for all (x) concentration. It is obvious that the zero frequency limits $\epsilon_1(0)$ is an essential quantity, which represents the dielectric response to the static electric field.

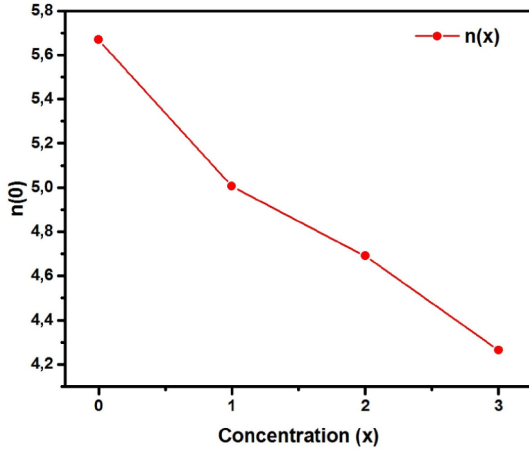


Figure 11. The static refractive index $n(0)$ versus composition (x).

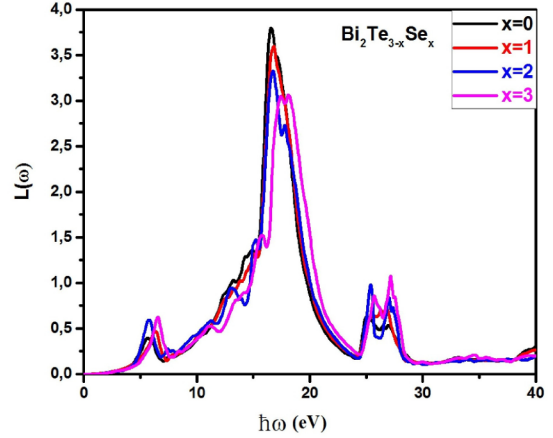


Figure 14. Energy loss function of $\text{Bi}_2\text{Te}_{3-x}\text{Se}_x$

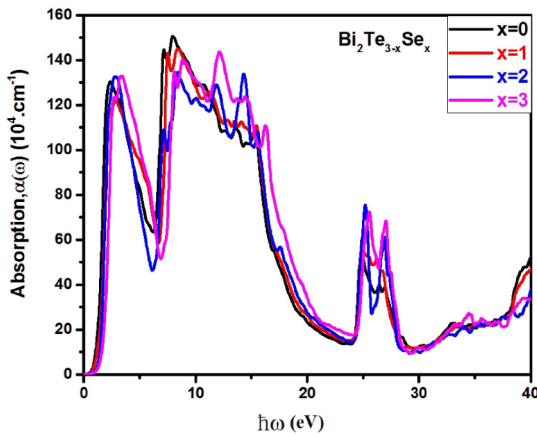


Figure 12. Absorption coefficient for $\text{Bi}_2\text{Te}_{3-x}\text{Se}_x$

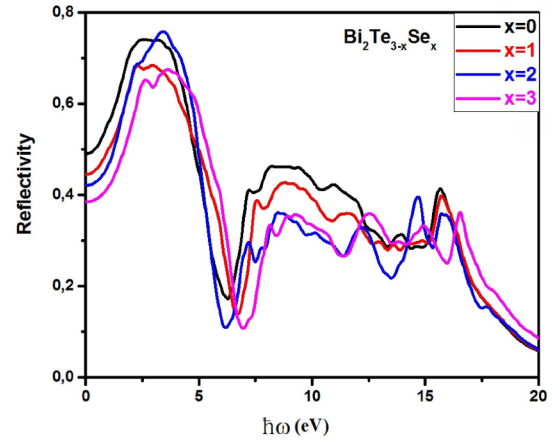


Figure 15. Reflectivity coefficient of $\text{Bi}_2\text{Te}_{3-x}\text{Se}_x$

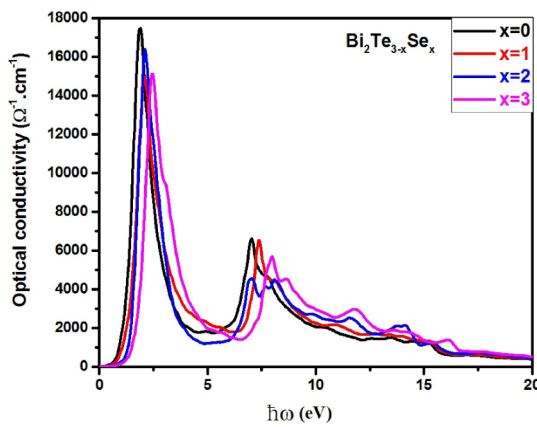


Figure 13. The optical conductivity of $\text{Bi}_2\text{Te}_{3-x}\text{Se}_x$

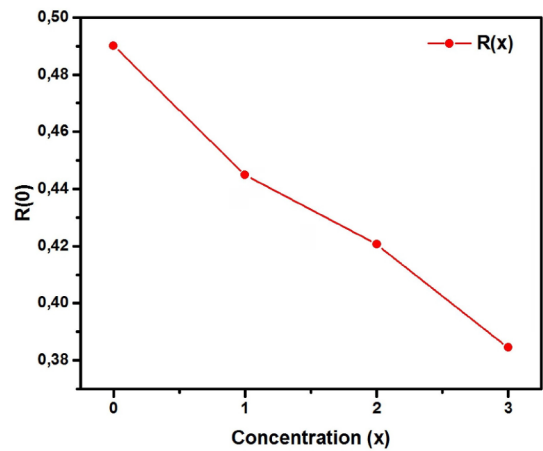


Figure 16. Reflectivity static versus concentration (x).

The static dielectric constants of the $\text{Bi}_2\text{Te}_{3-x}\text{Se}_x$ alloys at considered selenide (Se) compositions ($x=0, 1, 2$ and 3) are 32.1261, 25.0579, 21.9968 and 18.1802, respectively. Fig. 6 again expose the main peaks are placed at 1.3741 eV, 1.5918 eV, 1.6462 eV and 1.9728 eV comparable to $x = 0$,

1, 2 and 3 respectively, revealing the peak moves toward the higher energy side with x increasing. Fig. 7 indicate the zero frequency limits $\epsilon_1(0)$ versus Se (selenide) concentration (x) with comparable data¹⁰. The bowing parameter of The static dielectric constants (the zero frequency limits) $\epsilon_1(0)$

is determined by fitting the non linear variation, Relation (13) show the result:

$$\epsilon_1^{\text{Bi}_2\text{Te}_{3-x}\text{Se}_x}(0) = 31.88797 - 6.92858x + 0.8129x^2 \quad (13)$$

The imaginary part of the dielectric function of $\text{Bi}_2\text{Te}_{3-x}\text{Se}_x$ alloys with different concentration (x) is illustrated by Fig. 8. Our investigations of the imaginary part of the dielectric function trajectory exhibit that the first critical point of the dielectric function at $x=0, 1, 2$ and 3 exist about 0.4489 eV, 0.5306 eV, 0.8843 eV and 1.02 eV, respectively. It is visible that the critical point change toward higher energies with the increase of Selenide concentration. With rising energy, we sign that the dielectric function $\epsilon_2(\omega)$ display a essential maximum located at 1.8367 eV, 2.0272 eV, 2.0816 and 2.4082 eV for $x=0, 1, 2$ and 3 , respectively. When the Selenide composition increase, all the structures in $\epsilon_2(\omega)$ are shifted toward higher energies.

The refractive index can provide information for us about the behavior of light. When light passes through the different substances its velocity decreases by increasing of the refractive index of these substances. In Fig.9, the refractive index shows an appreciable value in low-energy region and a considerable reduction in high-energy region.

In Fig. 9 and 10, we show the refractive index $n(\omega)$ and the extinction coefficient $k(\omega)$ of $\text{Bi}_2\text{Te}_{3-x}\text{Se}_x$ with different composition (x) at the equilibrium lattice constant were calculated using TB-mBJ method. From Fig. 9 we can detect that the static refractive index $n(0)$ for Bi_2Te_3 , $\text{Bi}_2\text{Te}_2\text{Se}$, Bi_2TeSe_2 and Bi_2Se_3 are found to be 5.6685 , 5.0061 , 4.6903 and 4.2640 , respectively. Fig. 11 exhibit the static refractive index $n(0)$ versus composition (x). The bowing parameter of The static refractive index $n(0)$ is determined by fitting the non linear variation, Relation (14) exhibit the result. The $n(\omega)$ present a crucial maximum located at 1.5374 eV, 1.7551 eV, 1.7007 eV and 2.1360 eV for $x=0, 1, 2$ and 3 , respectively.

$$n^{\text{Bi}_2\text{Te}_{3-x}\text{Se}_x}(0) = 5.6456 - 0.6299x + 0.0590x^2 \quad (14)$$

The absorption coefficient $\alpha(\omega)$ is presented in Fig. 12, is an important parameter of each optoelectronic devices. The spectrum of absorption demonstrates that the energy of the threshold using TB-mBJ method is around 1.2088 eV for Bi_2Te_3 , 1.4059 eV for $\text{Bi}_2\text{Te}_2\text{Se}$, 1.4615 eV for Bi_2TeSe_2 and 1.7601 eV for Bi_2Se_3 with x varies from 0 to 3 , this energy is called the threshold of absorption. Each peak corresponds to an electronic transition, the first peak is located at around 2.3537 eV, 2.8708 eV, 2.7891 eV and 3.4150 eV for Bi_2Te_3 , $\text{Bi}_2\text{Te}_2\text{Se}$, Bi_2TeSe_2 and Bi_2Se_3 respectively, these energies are corresponding to the visible field except Bi_2Se_3 which is conform to the Ultraviolet range.^{42,43} The maximum of all peaks in the absorption curve is located, at 7.9321 eV for Bi_2Te_3 , surroundings 8.4219 eV for both $\text{Bi}_2\text{Te}_2\text{Se}$, and Bi_2TeSe_2 and 12.1220 eV for Bi_2Se_3 . Be accordant

to the corresponding wavelength of these energies, we can remark that these materials are good applicant to work into Ultraviolet fields; in addition the absorption curve becomes considerable according to the Selenide composition; it amount its maximum in the Ultraviolet field. These advantage us to glean that these components can produce as absorption components of the Ultraviolet waves.

The optical conductivity presented and described as a function of inter-band and intra-band transitions. Figure 13 shows the optical conductivity $\sigma(\omega)$ of $\text{Bi}_2\text{Te}_{3-x}\text{Se}_x$ for a different concentration (x), sharp peak is visible for every Selenide (Se) composition located at 1.8911 eV, 2.0816 eV, 2.1088 eV and 2.4354 eV for Bi_2Te_3 , $\text{Bi}_2\text{Te}_2\text{Se}$, Bi_2TeSe_2 and Bi_2Se_3 respectively.

Fig. 14, show the loss function $L(\omega)$ for $\text{Bi}_2\text{Te}_{3-x}\text{Se}_x$ for ($x=0,1,2$ and 3). The peak of the loss function reflects the characteristic associated with plasma oscillation; the corresponding oscillation frequency is called plasma frequency. There is no distinct peak at energies below 5 eV and more than 28 eV. Pointed summit situated at 16.65 eV for Bi_2Te_3 , $\text{Bi}_2\text{Te}_2\text{Se}$, Bi_2TeSe_2 and 18.1363 eV for Bi_2Se_3 .

The reflectivity coefficient for $\text{Bi}_2\text{Te}_{3-x}\text{Se}_x$ is shown in Fig. 15. The importance peaks in reflectivity are product from interband transitions. In very low energies, reflectivity is about 49.01% , 44.49% , 42.06% and 38.45% for Bi_2Te_3 , $\text{Bi}_2\text{Te}_2\text{Se}$, Bi_2TeSe_2 and Bi_2Se_3 respectively. Reflectivity reaches a peak around 74% , 68.34% , 75.78% and 67.45% for Bi_2Te_3 , $\text{Bi}_2\text{Te}_2\text{Se}$, Bi_2TeSe_2 and Bi_2Se_3 at the energy of 2.6256 eV, 2.8980 eV, 3.4150 eV and 3.6055 eV respectively, also, it is shown that after 18.57 eV the reflectivity decreases dramatically and tends towards zero. The bowing parameter of The static reflectivity constants (the zero frequency limits) $R(0)$ is determined by fitting the non linear variation, Relation (15) show the result:

$$R(0) = 0.4884 - 0.0409x + 0.0022x^2 \quad (15)$$

Our results exhibit a negligible bowing parameter for the static reflectivity constant $R(0)$, which has a bowing parameter $b = 0.0022$.

4. Conclusion

Bi_2Te_3 , $\text{Bi}_2\text{Te}_2\text{Se}$, Bi_2TeSe_2 and Bi_2Se_3 by means of Wien2K computational package, PBE-GGA, and TB-mBJ in the scheme of Density Function Theory, are studied to predict the structural, electronic and optical properties. The lattice constants a , c , the bulk modulus B and its pressure derivative B' of $\text{Bi}_2\text{Te}_{3-x}\text{Se}_x$ as a function of selenide concentration (x) ($x=0,1,2$ and 3) are calculated. The band structure of $\text{Bi}_2\text{Te}_{3-x}\text{Se}_x$ is calculated using GGA-PBE and TB-mBJ method, the result exhibit that for all concentrations have direct band gap. The real part $\epsilon_1(\omega)$, imaginary part of the dielectric function $\epsilon_2(\omega)$, refractive index $n(\omega)$, extinction coefficient $k(\omega)$,

absorption coefficient $\alpha(\omega)$, optical conductivity $\sigma(\omega)$, loss energy function $L(\omega)$ and the reflectivity $R(\omega)$ are calculated using both GGA-PBE and TB-mBJ.

Our results show that $\text{Bi}_2\text{Te}_{3-x}\text{Se}_x$ alloys are promising candidates for optoelectronic applications especially in the Infrared and visible fields. $\text{Bi}_2\text{Te}_{3-x}\text{Se}_x$ materials have a direct band gap and can be tuned from 0.1706 eV to 0.7819 eV by varying In composition so emission was tunable from 1.58 to 7.26 micrometers (infrared field), in addition for their direct band gap and in view of their attractive optical properties such conductivity, absorption and reflectivity these materials is considered as promising materials for optoelectronic applications as photodetector and Infrared Receivers.

5. References

- Bates CW, England L. An electron-mirror infrared image converter using vitreous selenium-bismuth photoconducting layers. *Applied Physics Letters*. 1969;14(15):390.
- Polvani DA, Meng JF, Chandra Shekar NV, Sharp J, Badding JV. *Chemistry of Materials*. 2001;13(6):2068-2071.
- Ovsyannikov SV, Shchennikov VV, Vorontsov GV, Manakov AY, Likhacheva AY, Kulbachinski VA. Giant improvement of thermoelectric power factor of Bi_2Te_3 under pressure. *Journal of Applied Physics*. 2008;104(5):053713.
- Ni HL, Zhao XB, Zhu TJ, Ji XH, Tu JP. Synthesis and thermoelectric properties of Bi_2Te_3 based nanocomposites. *Journal of Alloys and Compounds*. 2005;397(1-2):317-321.
- Cao YQ, Zhu TJ, Zhao XB. Thermoelectric Bi_2Te_3 nanotubes synthesized by low-temperature aqueous chemical method. *Journal of Alloys and Compounds*. 2008;449(1-2):109-112.
- Augustine S, Ampili S, Kang JK, E Mathai E. Structural, electrical and optical properties of Bi_2Se_3 and $\text{Bi}_2\text{Se}_{(3-x)}\text{Te}_x$ thin films. *Materials Research Bulletin*. 2005;40(8):1314-1325.
- Scheele M, Oeschler N, Meier K, Kornowski A, Klinke C, Weller H. Synthesis and thermoelectric characterization of Bi_2Te_3 nanoparticles. *Advanced Functional Materials*. 2009;19(21):3476-3483.
- Sharma Y, Srivastava P, Dashora A, Vadkhiya L, Bhayani MK, Jain R, et al. Electronic structure, optical properties and Compton profiles of Bi_2S_3 and Bi_2Se_3 . *Solid State Sciences*. 2012;14(2):241-249.
- Yu Y, Sun WT, Hu ZD, Chen Q, Peng LM. Oriented Bi_2Se_3 nanoribbons film: Structure, growth, and photoelectric properties. *Materials Chemistry and Physics*. 2010;124(1):865-869.
- Rahnamaye Aliabad HA, Kheirabadi M. Thermoelectricity and superconductivity in pure and doped Bi_2Te_3 with Se. *Physica B: Condensed Matter*. 2014;433:157-164.
- Zhao K, Wang Y, Xin C, Sui Y, Wang X, Wang Y, et al. Pressure-induced anomalies in structure, charge density and transport properties of Bi_2Te_3 : A first principles study. *Journal of Alloys and Compounds*. 2016;661:428-434.
- Wiese JR, Muldrew L. Lattice constants of Bi_2Te_3 - Bi_2Se_3 solid solution alloys. *Journal of Physics and Chemistry of Solids*. 1960;15(1-2):13-16.
- Nechaev IA, Hatch RC, Bianchi M, Guan D, Friedrich C, Aguilera I, et al. Evidence for a direct band gap in the topological insulator Bi_2Se_3 from theory and experiment. *Physical Review B*. 2013;87(12):121111.
- Austin IG. The Optical Properties of Bismuth Telluride. *Proceedings of the Physical Society*. 1958;72(4):545.
- Kohn W, Sham LJ. Self-Consistent Equations Including Exchange and Correlation Effects. *Physical Review*. 1965;140(4A):A1133.
- Perdew JP, Burke K, Ernzerhof M. Generalized Gradient Approximation Made Simple. *Physical Review Letters*. 1996;77(18):3865.
- Tran F, Blaha P. Accurate Band Gaps of Semiconductors and Insulators with a Semilocal Exchange-Correlation Potential. *Physical Review Letters*. 2009;102(22):226401.
- Blaha P, Schwarz K, Madsen GKH, Kvasnicka D, Luitz J. WIEN2K: An Augmented Plane Wave and Local Orbitals Program for Calculating Crystal Properties. Vienna: Vienna University of Technology; 2001.
- Kurth S, Perdew JP, Blaha P. Molecular and solid-state tests of density functional approximations: LSD, GGAs, and meta-GGAs. *International Journal of Quantum Chemistry*. 1999;75(4-5):889-909.
- Staroverov VN, Scuseria GE, Tao J, Perdew JP. Tests of a ladder of density functionals for bulk solids and surfaces. *Physical Review B*. 2004;69(7):075102.
- Yassin OA. Electronic and optical properties of $\text{Zn}_0.75\text{Cd}_0.25\text{S}_1-z\text{Se}_z$ first-principles calculations based on the Tran-Blaha modified Becke-Johnson potential. *Optik - International Journal for Light and Electron Optics*. 2016;127(4):1817-1821.
- Najwa Anua N, Ahmed R, Shaari A, Saeed MA, Haq BU, Goumri-Said S. Non-local exchange correlation functionals impact on the structural, electronic and optical properties of III-V arsenides. *Semiconductor Science and Technology*. 2013;28(10):105015.
- Haq BU, Ahmed R, Hassan FEH, Khenata R, Kasmin MK, Goumri-Said S. Mutual alloying of XAs (X = Ga, In, Al) materials: Tuning the optoelectronic and thermodynamic properties for solar energy applications. *Solar Energy*. 2014;100:1-8.
- Tran F, Blaha P, Schwarz K. Band gap calculations with Becke-Johnson exchange potential. *Journal of Physics: Condensed Matter*. 2007;19(19):196208.
- Murnaghan FD. The Compressibility of Media under Extreme Pressures. *Proceedings of the National Academy of Sciences of the United States of America*. 1944;30(9):244-247.
- Barnes JO, Rayne JA. Lattice expansion of Bi_2Te_3 from 4.2 K to 600 K. *Physics Letters A*. 1974;46(5):317-318.
- Francombe MH. Structure-cell data and expansion coefficients of bismuth telluride. *British Journal of Applied Physics*. 1958;9(10):415.
- Huang BL, Kaviani M. Ab initio and molecular dynamics predictions for electron and phonon transport in bismuth telluride. *Physical Review B*. 2008;77(12):125209.
- Sokolov OB, Skipidarov SY, Duvankov NI, Shabunina GG. Phase relations and thermoelectric properties of alloys in the Bi_2Te_3 - Bi_2Se_3 system. *Inorganic Materials*. 2007;43(1):8-11.

30. Wyckoff RWG. *Crystal Structures*. 2nd ed. New York: John Wiley and Sons; 1963.
31. Chen X, Zhou HD, Kiswandhi A, Miotkowski I, Chen YP, Sharma PA, et al. Thermal expansion coefficients of Bi_2Se_3 and Sb_2Te_3 crystals from 10 K to 270 K. *Applied Physics Letters*. 2011;99(26):261912.
32. Zimmer A, Stein N, Johann L, Van Gils S, Terryn H, Stijns E, et al. Infrared and Visible Dielectric Function of Electroplated $\text{Bi}_{2-x}\text{Te}_{3+x}$ Films Determined by Spectroscopic Ellipsometry. *Journal of the Electrochemical Society*. 2005;152(10):G772-G777.
33. Köhler H. Non-Parabolicity of the Highest Valence Band of Bi_2Te_3 from Shubnikov-de Haas Effect. *Physica Status Solidi B*. 1976;74(2):591-600.
34. Köhler H. Non-Parabolic $E(k)$ Relation of the Lowest Conduction Band in Bi_2Te_3 . *Physica Status Solidi B*. 1976;73(1):95-104.
35. Black J, Conwell EM, Seigle L, Spencer CW. Electrical and optical properties of some $\text{M}_2^{\text{v-b}}\text{N}_3^{\text{vi-b}}$ semiconductors. *Journal of Physics and Chemistry of Solids*. 1957;2(3):240-251.
36. Mooser E, Pearson WB. New Semiconducting Compounds. *Physical Review*. 1956;101(1):492.
37. Kim M, Freeman AJ, Geller CB. Screened exchange LDA determination of the ground and excited state properties of thermoelectrics: Bi_2Te_3 . *Physical Review B*. 2005;72(3):035205.
38. Scheidemantel TJ, Ambrosch-Draxl C, Thonhauser T, Badding JV, Sofo JO. Transport coefficients from first-principles calculations. *Physical Review B*. 2003;68(12):125210.
39. Delin A, Ravindran P, Eriksson O, Wills JM. Full-potential optical calculations of lead chalcogenides. *International Journal of Quantum Chemistry*. 1998;69(3):349-358.
40. Alouani M, Wills J. Calculated optical properties of Si, Ge, and GaAs under hydrostatic pressure. *Physical Review B*. 1996;54(4):2480-2490.
41. Dressel M, Grüner G. *Electrodynamics of Solids: Optical Properties of Electrons in Matter*. Cambridge: Cambridge University Press; 2002.
42. Fox M. *Optical Properties of Solids*. Oxford: Oxford University Press; 2001.
43. Saha S, Sinha TP, Mookerjee A. Electronic structure, chemical bonding, and optical properties of paraelectric BaTiO_3 . *Physical Review B*. 2000;62(13):8828-8834.
44. Givens MP. Optical Properties of Metals. In: Seitz F, Turnbull D, eds. *Solid State Physics*. Volume 6. New York: Academic Press; 1958. p. 322.